

Dissolution of olivine in basaltic liquids: experimental observations and applications

CARL R. THORNER AND J. STEPHEN HUEBNER

*U. S. Geological Survey
Reston, Virginia 22092*

Abstract

Rates of olivine dissolution in synthetic lunar basalt 77115 and a silica-enriched 77115 composition (Sil-77115) at superliquidus temperatures have been determined. Polished olivine plates of known composition, orientation, and size were placed in basalt mixes contained in high-purity iron crucibles and heated in evacuated silica tubes. Olivine plates dissolve in the 77115 melt at rates of ~ 0.2 to $616 \mu\text{m/hr}$ over a temperature range of 1265° to 1450°C ; these rates are consistently faster in the more siliceous melt. Olivine resorption rates are independent of crystallographic orientation and run duration.

Dissolution-rate data have been applied to the problem of the thermal history of fragment-laden impact-melt rocks of the lunar highlands. On the basis of estimates of the survival time of angular olivine xenocrysts in lunar basalt 77115, we conclude that the impact melt cooled to near-liquidus temperatures ($\sim 1250^\circ\text{C}$) within 1 hour and that temperatures did not exceed 1450°C for more than several seconds or remain above 1315°C for longer than a few minutes. In addition, textural and chemical criteria for the recognition of olivine resorption (and growth) phenomena in igneous rocks are discussed.

Introduction

Olivine is a primary phase in a large variety of mafic and ultramafic magmas over a wide range of physical conditions. The prevalence of olivine in the earth's crust and upper mantle and its relatively simple crystal chemistry and structure have prompted multifarious investigations of its nature and occurrence, which in turn have provided some fundamental precepts of igneous petrology. Most notable among these studies are those on olivine solid solution and phase equilibria (Bowen and Schairer, 1935; Roeder and Emslie, 1974), diffusivity (Buening and Buseck, 1973) and electrical conductivity (Duba, 1976). This study addresses the kinetics of olivine dissolution in basaltic liquids. In addition to providing experimentally derived data on the rates at which olivine dissolves in basaltic host melts, we have resolved both textural and chemical criteria for olivine dissolution that can be applied to the recognition of resorption (and growth) phenomena in igneous rocks and hence to the interpretation of their petrogenetic histories.

Olivine dissolves in silicate melts in which it is unstable as a result of the mixing of olivine into hotter (relative to the olivine thermal-stability limit) magma or compositionally incompatible magma. These conditions are exemplified by the superheating of olivine-bearing basalt as a result of impact melting, the dynamic convection of a magma that crystallizes olivine and circulates it to hotter regions, the mixing of olivine-bearing melts of dissimilar composition or temperature, and the reaction of olivine with the fractionated product of its own parent magma.

Innovative experimental investigations of high-temperature melting processes of basaltic material include dynamic melting of lunar basalt (Lofgren et al., 1978) and measurement of the dissolution rates of coexisting garnet, pyroxene, and olivine in alkali-basalt melt at 14 kbar (Scarfe et al., 1980); and evaluation of the kinetics of crystal dissolution in the synthetic system diopside-forsterite-anorthite (Kuo, 1982). The original intent of our investigation was to set limits on the early thermal history of impact-melt rocks of the lunar highlands. These rocks are interpreted as having formed from sheets composed initially of superheated silicate liquid and cold clasts (including olivine fragments) that were incorporated in the melt during its rapid transport away from the point of meteoritic impact (Simonds, 1975). Fragment-laden pigeonite basalt 77115 collected at Station 7 during the Apollo 17 lunar excursion is such a rock. Precise limits on the cooling history from temperatures at which the host melt began to crystallize ($\sim 1230^\circ\text{C}$) have already been established by experimental reproduction of both matrix crystallization products and olivine xenocryst zonation via diffusive cation exchange with the crystallizing host (Thorner and Huebner, 1980; Sanford and Huebner, 1980).

The initial thermal equilibration of hot melt and cold clasts was considered by Onorato et al. (1978), who found that thermal equilibrium would be achieved within several minutes. However, our experiments and those of Lofgren et al. (1978) show clearly that chemical equilibrium is not achieved so quickly. Therefore, the degree of chemical disequilibrium between melt and suspended xenocrysts could limit interpretations of the early thermal history of the melt

sheets. Our present investigations address this period of time in the thermal history of 77115 by measuring dissolution rates for olivine and applying them to the olivine xenocryst "survival time" in the 77115 melt at superliquidus temperatures.

An additional application of the experimental data to terrestrial occurrences concerns the appearance of resorbed olivines in mixed-magma eruptions and Hawaiian lava lakes (see discussion). Robinson and Thornber (in prep.) present a theoretical treatment of the rates and mechanisms of olivine dissolution and comparisons of previously obtained dissolution rate data, which enhances the potential application of these data.

Experimental technique

Gem-quality olivine crystals (F_O₉₂), from the collection of one of us (JSH), and possibly from San Carlos, N. Mexico (compare compositions, Table 1), were oriented by the X-ray precession method and cut, while still mounted on the goniometer-head, into plates perpendicular to major crystallographic directions of the reciprocal lattice (i.e., a*, b* and c* being parallel to a, b and c). These plates were doubly polished and their dimensions were measured by means of a precision machinist's micrometer (±0.5 μm resolution) and microscopic techniques. Dimensions of the plates ranged from ~1.0 to 1.5 mm in length and ~0.5 to 1.0 mm width; each plate had a thickness held constant to ±0.005 mm in the range 0.21–0.43 mm. Olivines were placed in sintered glass having the composition (Table 1) of lunar basalt 77115 (Thornber and Huebner, 1980) or a silica-enriched 77115 mix (Sil-77115). The olivine/basalt weight ratio in these experiments averaged ~0.056. Details of the preparation of synthetic lunar basalt glasses and reduced starting material have been presented by Thornber and Huebner (1982).

Charges were contained in 1/4-in. (6.35 mm)-diameter crucibles of high-purity iron (Materials Research Corp. VP-grade lot #26/1926), which have been shown not to impart significant changes in charge bulk composition (Thornber and Huebner, 1982). Only two olivine-dissolution experiments (77115-78, -79; Table 2) were run using Armco¹ electromagnet-grade iron crucibles, which were pretreated in CO/CO₂ atmosphere at 1000°C for ~100 hrs. (Thornber and Huebner, 1982). Loaded and sealed crucibles were enclosed in evacuated silica tubes which were next heated, then annealed isothermally in vertical quench-type furnaces at temperatures above the liquidus of the basalt compositions. Temperatures of each run were continuously monitored by calibrated Pt₉₀Rh₁₀ thermocouples adjacent to the charge. The run assemblies were quenched by being dropped into water; then polished thin sections were made from slices through each charge that had been cut perpendicular (within 5°) to the partially dissolved olivine plate. The thicknesses of the olivine plates after heating were measured with a precision of (± ~0.002 mm) by means of a petrographic microscope with a calibrated micrometer eyepiece. Rates of olivine dissolution were then evaluated by measurement of the changes in olivine thickness with run time.

Olivine-saturation experiments were done to determine melt compositions in equilibrium with olivine at high temperatures above the melting point of both starting mixtures. Starting materi-

Table 1. Composition of starting material

Basalt Glass (thrice fused in air)										
	77115		Sil-77115							
No. Analyses	10		10							
Oxides	Wt. %	Std. dev.	Wt. %	Std. dev.						
SiO ₂	45.09	0.60	52.32	0.59						
TiO ₂	2.86	0.07	2.55	0.12						
Al ₂ O ₃	17.18	0.20	16.29	0.10						
FeO*	9.44	0.31	8.38	0.16						
O ₂ **	1.06	-	0.94	-						
MnO	0.02	0.01	0.01	0.02						
MgO	10.67	0.08	9.09	0.08						
CaO	12.00	0.13	9.59	0.18						
Na ₂ O	1.60	0.07	0.67	0.01						
K ₂ O	0.17	0.015	0.19	0.01						
Total	100.09		100.03							
Olivine										
	SSHP-1		SSHP-3		SSHP-7		San Carlos (DJS)			
No. Analyses	5		5		5		5			
Oxide	Wt. %	Std. dev.	Wt. %	Std. dev.	Wt. %	Std. dev.	Wt. %	Std. dev.		
SiO ₂	40.29	0.26	40.21	0.32	40.39	0.54	40.31	0.40		
TiO ₂	0.00	0.02	0.00	0.01	0.00	0.01	0.03	0.02		
Cr ₂ O ₃	0.00	0.02	0.01	0.01	0.00	0.00	0.01	0.01		
NiO	0.35	0.04	0.42	0.03	0.35	0.03	0.38	0.04		
FeO*	9.50	0.05	8.46	0.05	9.43	0.07	8.82	0.40		
MnO	0.03	0.02	0.00	0.01	0.00	0.00	0.00	0.00		
MgO	49.76	0.09	50.69	0.10	49.64	0.24	50.44	0.63		
CaO	0.00	0.00	0.00	0.00	0.00	0.00	0.04	0.01		
Total	99.93		99.79		99.81		100.03			

*all iron recalculated as FeO
**excess oxygen, assuming all iron is ferric

als for these runs were 2/3 by weight of basalt mix (of 77115 or Sil-77115 composition) and 1/3 of <200 mesh separate of olivine known to be from San Carlos (Table 1). The experiments were run according to the technique described above. Table 3 gives the compositions of liquids saturated with olivine at various temperatures.

Major- and minor-element compositions of starting materials and run products were determined by electron-microprobe analysis using either (1) an Applied Research Laboratories model EMX electron microprobe operating in wavelength-dispersive mode (Finger and Hadjidiacos, 1972) or in combined energy- and wavelength-dispersive modes (Wiggins and Huebner, 1981), or (2) an ARL-SEM-Q microprobe in wavelength-dispersive mode. Microprobe standards were Marjalahti Olivine (Yoder and Sahama, 1957) or glass standard VGA99 (Jarosewich et al., 1979). Nominal operating conditions were 15 kV and 0.100 μA beam current, with a 20-second count time. Data were reduced on line by the method of Bence and Albee (1968) with revised alpha factors of Albee and Ray (1970). Compositional profiles were measured using the ARL-EMX microprobe with a mechanically stepped stage axis, at the same nominal operating conditions, except that count times for traverse points were: 10 sec for Al, Mg, Ca, and Fe in basaltic glass; 5 seconds for Fe, Mg, and Si in olivine; and 60 sec for Ni in olivine. Raw-count data of profiles were converted to approximate

¹ Any use of trade names in this report is for descriptive purposes only and does not constitute endorsement by the U. S. Geological Survey.

Table 2. Summary of glass compositions and experimental run data

77115													
Run no.	78*	79*	80	83	84	85	86	89	90	91	92	93	94
No. analyses	3	4	4	3	3	4	3	3	3	3	3	3	3
Wt. %													
SiO ₂	44.52	46.21	44.74	44.76	45.70	45.84	45.10	47.02	44.33	47.24	46.82	47.28	45.8
TiO ₂	3.05	2.99	2.97	2.89	2.92	2.89	2.99	2.81	2.77	2.77	2.77	2.96	2.84
Al ₂ O ₃	17.13	17.56	17.39	16.88	17.21	16.95	17.32	18.51	18.43	18.15	18.15	18.69	18.2
"FeO"	10.66	5.87†	10.24	10.55	9.41	9.31	9.52	7.94	8.29	8.73	9.12	8.29	8.9
MgO	11.57	12.39	11.83	11.90	12.24	12.32	11.56	12.49	11.78	12.72	12.62	11.65	12.4
CaO	12.09	12.71	12.48	11.86	11.92	11.78	12.32	10.66	10.77	10.56	10.38	10.84	10.8
Na ₂ O	1.47	1.35	0.94	1.00	1.38	1.32	1.33	0.79	0.77	0.72	0.72	0.69	0.63
K ₂ O	0.21	0.13	0.07	0.15	0.16	0.16	0.18	0.20	0.21	0.19	0.18	0.18	0.15
Total	100.70	99.21	100.66	99.99	100.94	100.57	100.32	100.42	99.35	101.08	100.76	100.58	99.72
Temp, °C	1265	1263	1265	1275	1297	1326	1280	1265	1266	1330	1330	1285	1285
Time (hrs)	24	168	120.5	24	3.5	2.0	5.5	118	91.25	2.2	2.0	6.5	6.5
Olivine Plate no.	11V	1aV	1aVIII	1aXII	3aI	3aII	3aIII	3cIII	3bII	3bIII	3cIII	3bVI	3cIV
Orientation	⊥ a*	⊥ a*	⊥ a*	⊥ a*	⊥ a*	⊥ a*	⊥ a*	⊥ c*	⊥ b*	⊥ b*	⊥ c*	⊥ b*	⊥ c*
Orig. thickness (μm)	273	280	274	224	288	287	277	339	436	434	325	428	350
Max. final thickness, (μm)	252	210	NM	0	240	210	240	240	354	350	228	348	294
Min. resorb. rate (μm/hr)**	0.44	0.21	-	>4.7	6.9	19.3	3.4	0.42	0.45	18.0	24.3	6.2	4.3
Cusp wavelength (μm)	24	24	48-54	-	15	0	16	36	12-24	0	0	18	23
MgO+FeO/2 SiO ₂ (mole%)	0.293	0.252	0.292	0.296	0.286	0.285	0.279	0.268	0.264	0.274	0.282	0.256	0.283

77115					Si1-77115								
95	96	97	98	99	Si6*	Si11	Si16	Si17	Si18	Si19	Si20		
3	3	3	5	5	3	3	3	3	3	3	3		
SQ	FQ	FQ	SQ	FQ									
Wt. %												Wt. %	
46.70	46.70	46.05	45.68	46.49	52.56	52.54	53.69	53.53	52.34	52.67	51.99		
2.68	2.71	2.75	2.65	2.71	2.35	2.28	2.82	2.63	2.53	2.57	2.51		
18.10	18.24	18.30	17.62	18.15	15.95	15.76	16.03	16.48	15.88	16.27	15.60		
9.17	9.13	9.62	9.37	9.23	9.10	7.84	7.02	7.15	7.97	8.00	7.91		
12.20	11.77	11.82	13.48	13.04	9.60	11.17	10.93	9.60	10.51	9.79	11.46		
10.46	10.55	10.53	10.21	10.17	9.19	9.20	9.18	9.87	9.07	9.48	9.37		
0.77	0.81	0.82	0.75	0.80	0.68	0.49	1.34	0.58	0.65	0.68	0.58		
0.18	0.19	0.18	0.21	0.24	0.17	0.11	0.13	0.15	0.19	0.18	0.18		
100.26	100.10	100.07	99.97	100.83	99.60	99.49	101.14	99.99	99.14	99.64	99.60		
1315	1315	1450	1450	1450	1240	1250	1240	1211	1315	1270	1284		
3.0	3.0	0.25	0.25	0.17	24	147.5	48	24.75	1.5	4.0	3.5		
3bIV	3cVIII	7I	7II	7III	1aIV	1aIX	1aXI	1aXIII	3cVI	3cV	3bVI		
⊥ b*	⊥ c*	-	-	-	⊥ a*	⊥ a*	⊥ a*	⊥ a*	⊥ c*	⊥ c*	⊥ b*		
429	323	244	398	400	267	218	208	214	345	365	415		
294	210	0	90	NM	162	0	138	Opx mantle	240	306	354		

Table 2. (cont.)

22.6	19.1	>488.0	616.0	-	2.2	>0.7	0.84	-	35.0	7.3	8.8
1-3	1-3	-	-	-	1	-	0	-	-	0	0
0.276	0.270	0.278	0.305	0.292	0.209	0.208	0.207	0.190	0.213	0.202	0.22

*Runs in CO/CO₂ pretreated Armco electromagnet-grade iron crucibles
†FeO loss due to run duration exceeding those of crucible pretreatment (see Thornber & Huebner, 1982)
FQ Fast Quench (see text)
SQ Slow Quench (see text)
NM not measured
** (Orig. thickness - max. final thickness) hr⁻¹ /2

weight-percent oxides, assuming a linear relationship between counts above background and concentration.

Results

Olivine dissolution rates

Table 2 presents a detailed summary of run data for experiments in which olivines were partially (or totally) resorbed in melt at temperatures exceeding the liquidus of the initial compositions of the two host liquids. Obvious differential resorption of plates in *one* experiment was inferred to have resulted from convection of melt within the 1/4 in. (6.35 mm) iron-crucible. This phenomenon is illustrated in Figure 1 (Run 85, 1326°C, 2 hrs) in which convective motion of the 77115 melt above the submerged olivine is indicated by: (1) preferential dissolution in the center of the plate; (2) the distribution of fine metallic Fe precipitate in a pattern reflecting convective flow above the olivine; and (3) the existence of large blebs of metallic Fe, which dangle from beneath the plate and which seem to have coalesced in a stagnant liquid. Possible differential resorption due to convection, plus the fact that plate edges tend to disappear faster than planar surfaces in all runs, prompted our decision to calculate the rate of dissolution as a minimum, using the maximum final thickness of olivine observed in multiple sections of each charge.

The minimum dissolution-rate-versus-temperature relationships for isothermal resorption of olivine in 77115 and Sil 77115 are presented in Figure 2. As anticipated, the olivine dissolution rate in basaltic melts increases with temperature, and the rates of resorption are consistently greater in the more siliceous melt. At ~15°C above the olivine (primary) liquidus temperature of 77115 melt, rates of olivine dissolution are <1 μm/hr, whereas at ~200°C above the liquidus, olivine dissolves at a rate of 488–616 μm/hr. In the Sil-77115 composition, rates are comparatively faster at all but low temperatures (Run 17), where olivine, which is in reaction relationship with pyroxene, is mantled by a dense aggregate of small euhedral crystals of pyroxene projecting from the interface into the melt. This mantle of pyroxene crystals would inhibit dissolution by isolating the olivine from the melt.

The rates of olivine dissolution appear independent of crystallographic orientation, unlike other properties of olivine, including chemical diffusion (Buening and Buseck, 1973), which are anisotropic.

In runs at ~1265°C in the 77115 melt composition, ranging in duration from 24 to 118 hours (Table 2, runs 78, 89, 90), a relatively constant dissolution rate was determined, indicating that isothermal resorption is not a time-dependent process. The anomalously low rate of resorption in run 79 (1265°C, 120.5 hours) is interpreted as having been the result of FeO loss from the charge (Table 2), because of a run duration that exceeded the pretreatment time of the electromagnet-grade iron crucible (Thornber and Huebner, 1982). This relatively constant dissolution rate was not unexpected because the large weight-percent ratio of melt to olivine precluded a significant change in the bulk melt composition.

Table 3. Composition and run data for olivine saturation experiments

Run no.	01 + 77115-1		01 + 77115-2		01 + Sil 77115-1		01 + Sil 77115-2	
No. Analysis	3		5		3		3	
Oxides	Wt. %	S.D.	Wt. %	S.D.	Wt. %	S.D.	Wt. %	S.D.
SiO ₂	46.95	0.35	47.07	0.29	51.97	0.87	50.93	0.50
TiO ₂	2.54	0.02	2.73	0.05	2.44	0.08	2.00	0.07
Al ₂ O ₃	16.83	0.05	18.30	0.08	16.50	0.11	13.24	0.12
"FeO"	9.04	0.11	8.40	0.14	6.79	0.15	7.54	0.12
MnO	0.09	0.01	0.08	0.02	0.09	0.01	0.08	0.03
MgO	15.30	0.11	13.13	0.14	12.77	0.05	18.05	0.30
CaO	10.02	0.09	10.56	0.23	9.67	0.13	7.64	0.10
Na ₂ O	0.50	0.01	0.75	0.01	0.22	0.01	0.39	0.03
K ₂ O	0.15	0.02	0.20	0.03	0.18	0.02	0.08	0.01
Total	101.42		101.22		100.63		99.95	
Temp. (°C)	1315		1275		1250		1350	
Time (hrs)	24		22		67		50	
MgO+FeO/2 SiO ₂ (mole %)	0.323		0.282		0.238		0.326	

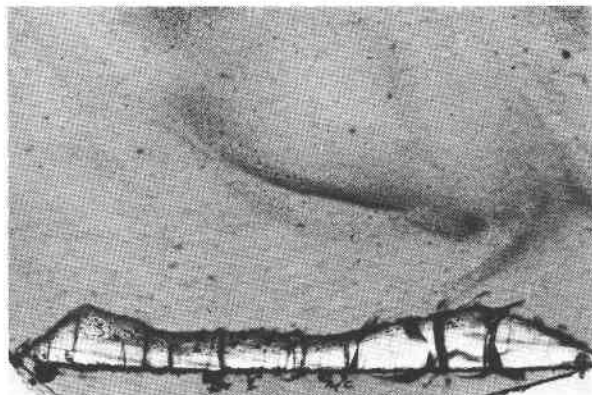


Fig. 1. Transmitted light photomicrograph of differentially resorbed olivine in 77115 melt (see text). Run 85, width of field = 2.19 mm.

Electron-microprobe compositional variations in bulk liquids, in glass adjacent to olivine, and in olivine

Bulk compositions of the quenched melt in each resorption run are presented in Table 2. These data are plotted in an olivine-basalt pseudo-binary diagram (Fig. 3) along with the composition of olivine, starting basalts, and olivine-saturated basalts. Because of the low olivine/basalt weight ratio, the compositions of the liquids in the experimental runs experienced only minimum changes as a result of partial or even complete dissolution of olivine plates. A minor increase in olivine component is sufficient to saturate the 77115 liquid with olivine at 1265°C. Despite the proximity to the saturation surface of compositions determined for olivine-dissolution experiments in 77115 melt at 1265°C, these runs show no evidence of any isothermal process other than resorption. The slight compositional overlap of

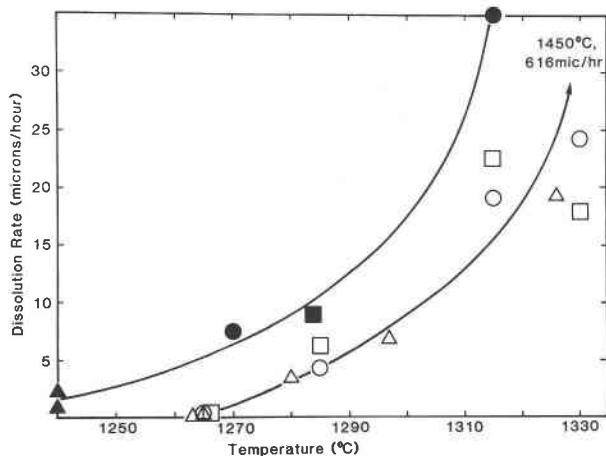


Fig. 2. Dissolution rate of olivine in 77115 (open symbols) and Sil 77115 (closed symbols) melts vs. temperature. Triangles, squares, and circles represent measured rates perpendicular to a*, b* and c* crystallographic directions, respectively.

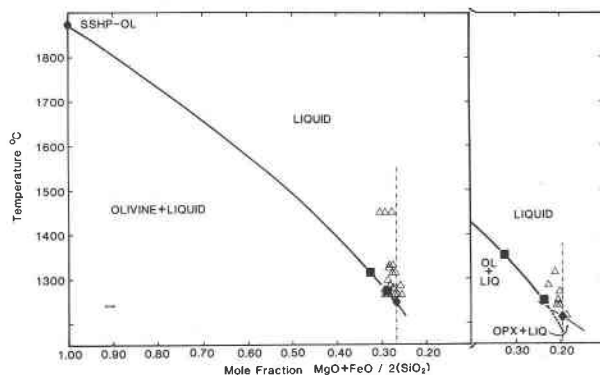


Fig. 3. Bulk liquids in olivine resorption experiments plotted in olivine-basalt pseudo-binary, illustrating olivine saturation surface as a function of temperature and mole fraction olivine component ($\text{MgO} + \text{FeO}/2 \text{SiO}_2$) between olivine and basalt compositions. For (a) (77115 run series) and (b) (Sil 77115 series) symbols are: closed diamonds—end-member olivine and basalts: 77115 precipitates olivine at its liquidus of 1249°C; Sil 77115 precipitates low Ca pyroxene (OPX) at 1205°C; melting point of olivine (FO_{92}) determined from data of Bowen and Schairer (1935), closed squares—Bulk glass composition in end-member basalts saturated with olivine (Table 3), open triangles—Bulk glass composition in olivine resorption experiments (Table 2). Dashed-dotted line represents line of constant composition of the starting basalt. Solid curve represents olivine saturation surface and is dashed in the region of olivine metastability below the pyroxene saturation surface in Fig. 3b. The “error bar” in the lower left represents an average of the range of deviation from the mean of replicate analyses of each bulk liquid.

these glasses, relative to the saturation surface, probably results from analytical uncertainty. We assume that liquids surrounding olivines in all dissolution-rate experiments provided an essentially infinite sink for the dissolved olivine components.

Compositional traverses across the crystal/liquid interfaces and far (up to 200 μm) into surrounding melts were completed to resolve increased concentration of dissolved olivine components around partially resorbed crystals. Because dissolution rate would obviously depend (in part) upon the composition of the melt at the interface, we wanted to include this factor when interpreting our data. No such gradients were observed, but traverse data revealed that the glasses immediately surrounding the olivines are actually depleted in MgO and enriched in Al_2O_3 and CaO . This pattern is consistent with growth rather than dissolution of olivine. To prove that this pattern was associated with growth during quench, pairs of isothermal resorption experiments were run at 1315° and 1450°C. In each pair, one run was removed from the furnace and allowed to cool slowly in air and the other was quickly drop-quenched into a cool solution of $\text{NaCl} + \text{H}_2\text{O}$. Figure 4 presents a comparison of composition profiles across the crystal/liquid interface for runs that were slowly and rapidly cooled from 1315°C. The extent of depletion of

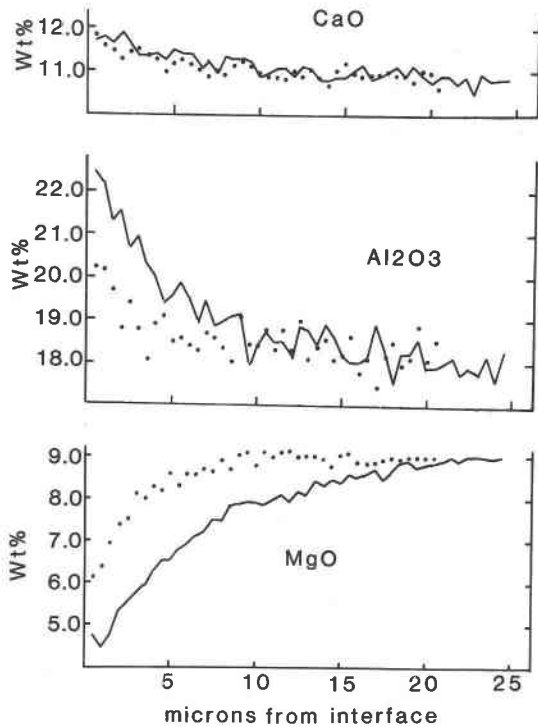


Fig. 4. Electron microprobe traverse data for glass adjacent to olivine in runs quenched slow (solid line) and fast (dotted line) from 1315°C (Runs 95 and 96, respectively). Weight percent oxide values in glass farthest from olivine are based on values given in Table 2 and the relative weight percent oxide values presented in the figure were approximated assuming linear correlation between counts above background on standards and unknown.

the MgO (olivine component) near the interface and the complementary enrichment of Al_2O_3 (excluded during olivine growth) is significantly greater in the slowly quenched run. CaO increases only slightly toward the interface in both experiments; The Ca pattern may reflect a relatively greater mobility of Ca in the rapidly cooling melt (Powell et al., 1980). FeO traverses are ambiguous because of the presence of metallic Fe blebs at the olivine-liquid interface. Although the extent of zonation varies locally in any given run, the magnitude of the envelope of anomalous compositions surrounding resorbed olivine increases with the temperature from which runs were quenched (Fig. 5). In all runs, the amount of MgO depletion in liquid around resorbed olivine corresponds to growth of less than $1 \mu\text{m}$ of solid olivine. Only in runs quenched from 1450°C was quench growth actually observed (Fig. 6).

The composition of resorbed olivines remains unchanged from core to outermost rim except in those experiments of long duration (>90 hours) in 77115 melt. In runs of long duration at 1265°C, there is a slight MgO depletion and complementary FeO enrichment of the olivine rim, which is most extensive in experiments of longest duration. The

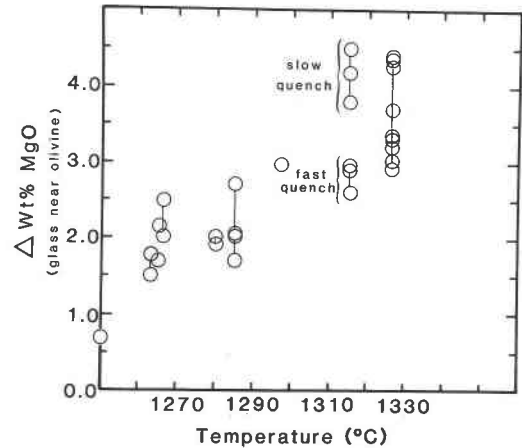


Fig. 5. Run temperature versus the maximum change in weight percent MgO in glass adjacent to resorbed olivine (relative to the bulk liquid) in all experiments; vertical lines connect data from different traverses of the same runs.

development of submicron-sized particles of Fe-Ni metal² (~25 wt.% Ni) within the olivine rims (Fig. 7a) complements the olivine compositional gradient in these runs. Electron-microprobe traverses of Ni in olivines in long runs at ~1265°C reveal Ni concentration profiles that show numerous and erratic spikes in olivine rims, which are the result of nickel-bearing metallic blebs precipitated within the olivine rim. This erratic variation in Ni content due to the metal blebs is superimposed on a pattern of Ni depletion in olivine as the rim is approached. In runs of short duration at higher temperatures, metallic precipitates are observed only in the outer 3–10 μm of resorbed olivine

² Ni-Fe precipitate identified by G. L. Nord (USGS) in the scanning transmission electron microscope by X-ray energy dispersive analysis.



Fig. 6. Extensive growth of olivine from resorbed olivine interface, outward into the 77115 liquid in run slowly quenched from 1450°C (highly reflective phase is Fe°). Run 98; reflected light; width of field = 0.55 mm.

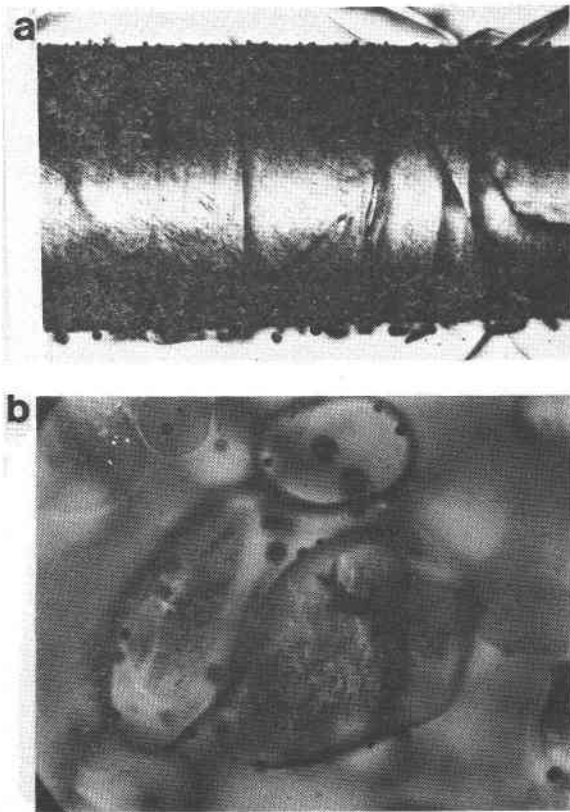


Fig. 7. Transmitted-light photomicrographs of olivines in resorption and saturation experiments. (a) Resorption run 90, heated for 91½ hours, showing rim containing Fe-Ni precipitate (opaque) and clean core; width of field = 0.71 mm. (b) Saturation run OL + Sil 77115-2, showing olivines with cores containing Ni-Fe precipitate (opaque) and clean rims; width of field = 0.22 mm.

rims (if at all). Olivine crystals present in charges saturated with olivine have an inverse core/rim relationship with regard to Ni-Fe precipitates (Fig. 7b) (i.e., olivine cores with precipitates are surrounded by clear olivine rims). The significance of the observed Fe-Ni precipitates in resorbed olivines is elaborated upon in the discussion.

Textural observations

Of especial significance to the practical application of our results is the characterization of textures at the interface between the melt and resorbed olivine. In addition to providing information relevant to the mechanism of olivine dissolution, these textures are basic criteria for recognizing resorption phenomena in igneous rocks.

Regularly spaced hummocks and valleys are characteristic of resorbed olivine surfaces in 77115 melt, as observed with the universal stage. These features appear as periodic cusps in cross section (Fig. 8a-c, f-h). These cusps form regardless of crystallographic orientation of the olivine surface and have a somewhat regular wavelength which gener-

ally increases with decreasing run temperature (Table 2). In contrast, olivines resorbed in the silica-enriched liquid have smooth surfaces or—at lower temperatures—very small cusps (Fig. 8d, e).

Blebs of metallic Fe are attached to the olivine in all experiments and are frequently concentrated in the vicinity of partially dissolved crystals (Fig. 8a-h). Blebs often occur at regular intervals in valleys or ridges of the olivine surface. They are occasionally positioned at “peaks” of olivine, where they appear to have impeded olivine/melt reaction. Scanning-electron-microscopy X-ray mapping revealed significant amounts of Ni in Fe blebs spatially associated with partially resorbed olivines. Metallic Fe blebs that do not occur in the vicinity of olivine are sporadically present in some charges and show no evidence of Ni concentration. These observations suggest that some metallic blebs form near the interface as a result of the process of olivine resorption. The relative concentration of Ni in these blebs may be due to the coalescence, at the resorbed interface, of Ni-rich Fe-metal precipitate produced within olivine rims, which would, in turn, tend to stabilize the metallic Fe phase under these f_{O_2} conditions and thus promote Fe precipitation from the liquid at the interface.

Discussion

The dissolution mechanism—a negative result

Our experimental results indicate that the rate of dissolution is not controlled by diffusion of olivine components from the interface through the melt. Dissolution controlled by diffusion of olivine components through the melt was modelled numerically by using a Fortran program (RESORB), which was prepared by modifying the PROG2 of Sanford (1982). A range of input factors (width of olivine and melt, concentration or activity of olivine components in crystalline olivine and in initial and saturated melts, diffusivity of olivine components in melt) was tested. Each model calculation resulted in a significant gradient that extended far into the melt (beyond the 15- to 30-micrometer envelope that develops during quenching). Each model also shows that, in a diffusion-controlled process, the dissolution rate as we express it decreases with time. Neither of these features, characteristic of a process controlled by diffusion in the melt, was found to be present in our experimental run products. We conclude that the dissolution process is not rate-limited by diffusion of olivine components in the melt and suggest instead that the rate is limited by some mechanism that operates at the interface. Possible mechanisms are the subject of a complementary paper by G. P. Robinson and Thornber (in prep.).

Glass compositional gradients—a caution

Obvious discrepancies in major-element-distribution coefficients between coexisting crystals and glasses have been attributed to quenching techniques, which are insufficiently rapid for preservation of the liquid as a glass of the same composition (Cawthorn et al., 1973). Depletion of olivine components in glass surrounding (or included in) olivine

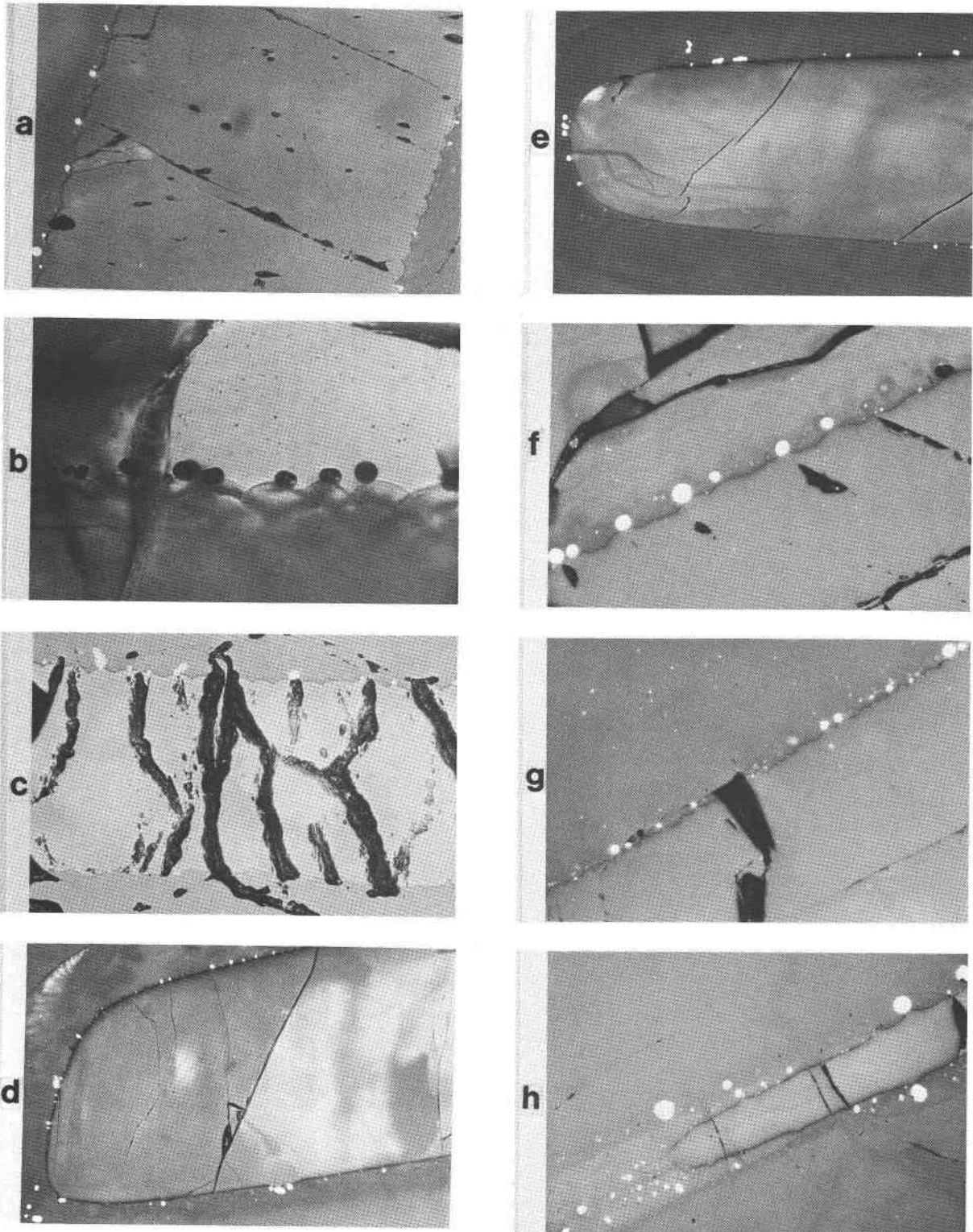


Fig. 8. Photomicrographs illustrating variations in texture of the resorbed olivine interface in experimental runs (see text). (a, c-h: reflected light, olivine is light grey, quenched liquid is dark grey and metallic iron is white. 8b, transmitted light, dark (lower) phase is olivine and blebs of metallic iron are opaque. Run numbers and widths of field are as follows: (a) 84, 0.36 mm; (b) 84, 0.14 mm; (c) 78, 0.55 mm; (d) Sil-8, 0.55 mm; (e) Sil 9, 0.55 mm; (f) 89, 0.44 mm; (g) 86, 0.36 mm; (h) 86, 1.11 mm.

crystals has been suggested as a result of quench overgrowth (Kushiro, 1974; Anderson, 1974; Cawthorn et al., 1973; Green, 1973). The ubiquitous presence of an "olivine-depleted" zone around isothermally resorbed olivine crystals in our experiments provides unique evidence for growth-related diffusion during quench. This explanation is substantiated by comparison of compositional profiles in similar runs quenched from successively higher temperatures and in runs quenched from the same nominal temperatures at variable rates (see results).

The gradients produced by quench growth of olivine in our experiments indicate that considerable caution must be used in calculating crystal-melt element distribution coefficients from adjacent analyzed points. Also, the efficiency of "quenching" must be taken into account when applying compositional gradients in glasses (adjacent to crystals) to an estimation of isothermal growth rate or element partitioning during growth or dissolution of the bulk of a crystalline phase.

Olivine resorption in terrestrial rocks

Partially resorbed crystalline phases in igneous rocks provide information relevant to the thermal and chemical history of magmas. We hope that our experimental data can be used to quantify the disequilibrium responsible for olivine dissolution in a rock and to yield definitive restrictions on its petrogenesis.

Despite the refractory nature of olivine, chemical and/or thermal disequilibrium between olivine and host melts is not uncommon in nature and results in partial olivine resorption. Lavas of the Medicine Lake Highlands, Calif. (Gerlach and Grove, 1982) contain millimeter-sized olivine phenocrysts with cusped and embayed margins, which are interpreted as having resulted from the mixing of chemically and thermally distinct magmas. In Kilauea Iki lava lake, Hawaii, resorbed olivines are found in core samples containing foundered, partially remelted crust and in olivine-rich diapirs that are driven upward into hotter parts of the lake (R. T. Helz, oral comm., 1982). Lavas of the 1959 summit eruption of Kilauea Volcano, Hawaii (which created Kilauea Iki lava lake), contain rounded and embayed olivine phenocrysts (0.5–5 mm) coexisting with smaller euhedral and skeletal phenocrysts of olivine (Richter and Murata, 1966). Wright (1973) has shown that the complex variation in bulk chemistry of the erupted lavas is a result of the mixing of compositionally distinct magmas. The magmas are interpreted as having been derived from two separate sources. These sources were initially tapped by spatially distinct fountains, which subsequently coalesced into a single flow of freshly blended basalt. We presume that resorption of olivine phenocrysts originally present in one of the source magmas resulted from the thermal and compositional incompatibility of this olivine with the hybridized host material. A detailed petrographic examination was made of olivine-bearing pumice samples from the 1959 Kilauea summit eruption. These samples were selected because of their extensive documentation and avail-

ability. Rounded olivine phenocrysts, present in specimens collected throughout the duration of this eruption, reveal a texture of periodic cusps along the crystal-liquid interface (Fig. 9). These cusps are similar to those observed in our experimental charges but have a greater wavelength. The observed similarity of textures associated with olivine dissolution in natural and experimental samples illustrates that they are not an experimental artifact and can be considered as a viable criterion for the recognition of resorption in igneous rocks.

Details of the specific nature of chemical and thermal disequilibria responsible for olivine dissolution in the 1959 Kilauea summit lavas have yet to be considered. As our experimental results indicate, the long cusp wavelength at the olivine-liquid interface is suggestive of a relatively low degree of host-melt superheating and a slow rate of dissolution in a melt that is relatively near the olivine-saturation surface.

The coexistence of resorbed olivine with a more fayalitic euhedral-skeletal olivine (Richter and Murata, 1966) supports this conclusion and is suggestive of the mixing of distinct magmas that were relatively compatible, as outlined by Wright (1973).

Fe-Ni precipitates in olivines "annealed" at high temperature and low total pressure

The formation of Fe-Ni precipitates within olivines subjected to heating in a silicate melt at ~ 1 atm. and low f_{O_2} may be the result of an intrinsic reduction of olivine containing carbon during heating at low pressures (Freund et al., 1980), or the result of an extrinsic reduction. Extrinsic reduction could be caused by the association of elemental carbon with the olivine (Sato, 1978) and/or by a product of a redox reaction between olivine and surrounding melt that is in equilibrium with metallic Fe. Textural observations of the Fe-Ni precipitate both in rims of experimentally re-

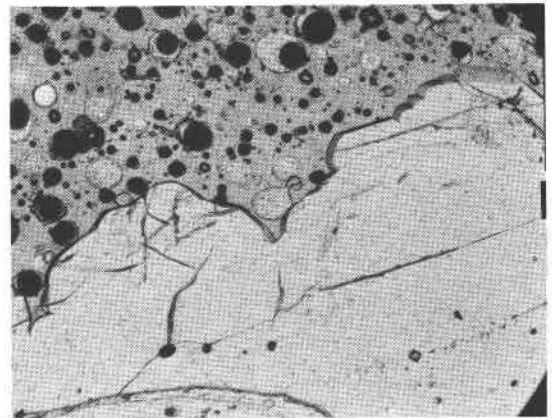


Fig. 9. Transmitted-light photomicrograph of resorbed olivine phenocrysts in pumice of Kilauea 1959 summit eruption (sample IKI-21); field of view = 1.11 mm. Dark round objects in glass are vesicles.

sorbed olivines and in cores of crystals in olivine-saturation experiments, indicate that more than one mechanism may be operative.

Fe-Ni precipitates in resorbed olivine rims (Fig. 7a) are similar to those observed by Boland and Duba (1981) in the rims of San Carlos olivine plates heated (in iron crucibles) in a reducing gaseous atmosphere at 950–1500°C (CO₂/H₂ or CO₂/CO mixtures defining an f_{O_2} lower than that defined by an olivine-pyroxene-Fe-gas assemblage). The precipitates in these experiments are interpreted as having formed as a result of gas-solid redox interaction at the interface. Because the penetration-depth of Fe-Ni metal in rims of our experimentally resorbed olivines is more extensive than that observed by Boland and Duba (J. N. Boland, pers. comm., 1982), solid-state reduction of olivine apparently proceeds faster in a metastable olivine-liquid system than in an olivine-gas system.

The "dirty" core-"clean" rim relationship of Ni-Fe precipitates in olivine crystals coexisting with olivine-saturated 77115 and Sil 77115 (Fig. 7b) may come about as a result of the subsequent growth of fresh olivine around the "seeds" of San Carlos olivine, which formed Fe-Ni either during initial equilibration with the silicate melt (+Fe^o) or after the nuclei were isolated from the melt by subsequent olivine overgrowth, by the mechanism of olivine "self-reduction" (Sato and Valenza, 1980). This texture is virtually identical with that observed by Rambaldi and Wasson (1982) in olivines of unequilibrated ordinary chondrites. We suggest that Fe-Ni precipitates in the meteoritic olivines may have formed during heating (or resorption) at low f_{O_2} and total pressure, thus reflecting conditions of the chondrite-forming event. These residual olivines subsequently served as nuclei for additional growth of olivine as "clear rims" from the surrounding partial melt.

The observed production of Fe-Ni precipitates in olivine, possibly by interplay of intrinsic and extrinsic reduction phenomena, may have a direct bearing on the genesis of similar intracrystalline precipitates in lunar samples (Haggerty, 1977) and terrestrial occurrences of Ni-Fe in association with serpentinized peridotites (Thorner and Haggerty, 1976).

Application of olivine-dissolution rates to the thermal history of lunar highlands impact-melt rock

Data on the rates of olivine dissolution in basaltic melt can be used to limit the possible interpretations of the early thermal history of impact-melt rocks of lunar highlands. When we combine results of this study with our previous experimental study of conditions required to reproduce crystallization and diffusion phenomena of fragment-laden basalt 77115 (Thorner and Huebner, 1980), we obtain a complete scenario for the thermal history of this rock type after the incorporation of its components. The thermal model involves rapid thermal equilibration of superheated melt and incorporated cold clasts during movement of the impact melt sheet away from its source (thermal regime #1), followed by cooling before (thermal regime #2) and

through (thermal regime #3) the crystallization interval (Fig. 10). Time-temperature profiles for each thermal regime were obtained from heat-flow equations for geometrically simple arrangements of hot and cold bodies (Onorato et al., 1978; Sanford and Huebner, 1980). The different rates for the early and the late stages of cooling come about because two different geometric scales were assumed to be involved. A rapid temperature equilibration between the superheated impact melt and small cold clasts over a small scale constitutes the initial thermal regime (#1); the rate of subsequent cooling is then dependent upon heat loss from the melt sheet to adjacent rock or cooler melt sheets (regimes #2,3).

Curves in thermal regime #3 (Fig. 10) are conductive cooling curves, which permit formation of observed zonation of olivine in 77115 basalt by a diffusion process (Sanford and Huebner, 1980). In our previous experimental study of the crystallization of 77115 (Thorner and Huebner, 1980), we found experimentally that the dashed curve best approximates the thermal history necessary to mimic the textures and mineralogy of the matrix and to reproduce the observed olivine xenocryst zonation via diffusive cation exchange with the crystallizing melt.

The filled circles of thermal regime #2 (Fig. 10) are based upon experimentally determined minimum rates of olivine dissolution and represent calculated time-temperature maxima for survival of sharp angular olivine xenocrysts (with <5 μm of rounding) in the 77115 melt. The early thermal history, after local thermal equilibrium between clasts and melt has been achieved, is therefore restricted to the range defined by the shaded region, within which a range of schematic cooling curves is shown. It is apparent that the melt cooled to near-liquidus temperature ($\sim 1250^\circ\text{C}$) within 1 hour. The temperature could not have exceeded 1450°C for more than a matter of seconds or remained above 1315°C for longer than a few minutes.

The presence in 77115 basalt of a few small ovoid olivine xenocrysts adjacent to sharp angular olivine fragments indicates that some melt must have existed at extreme temperatures long enough to cause appreciable resorption of some olivine fragments (thermal regime #1). Other lunar highlands melt rocks are compositionally and texturally heterogeneous. It seems likely that the first olivines incorporated in the superheated melt-sheet were partially dissolved and mechanically mixed with angular olivine fragments at some point farther from the source, and that the initial postemplacement cooling history for impact-melt rocks of the lunar highlands from superheated to sub-liquidus temperatures was extremely complicated.

Conclusions

In addition to the application of experimentally derived rates of olivine dissolution in basaltic liquids to the thermal history of lunar impact-melt rocks, results of this investigation are fortuitously pertinent to other petrologic phenomena:

1. The formation of metallic Fe-Ni precipitates in olivines annealed at 1 atm in silicate melts in equilibrium with

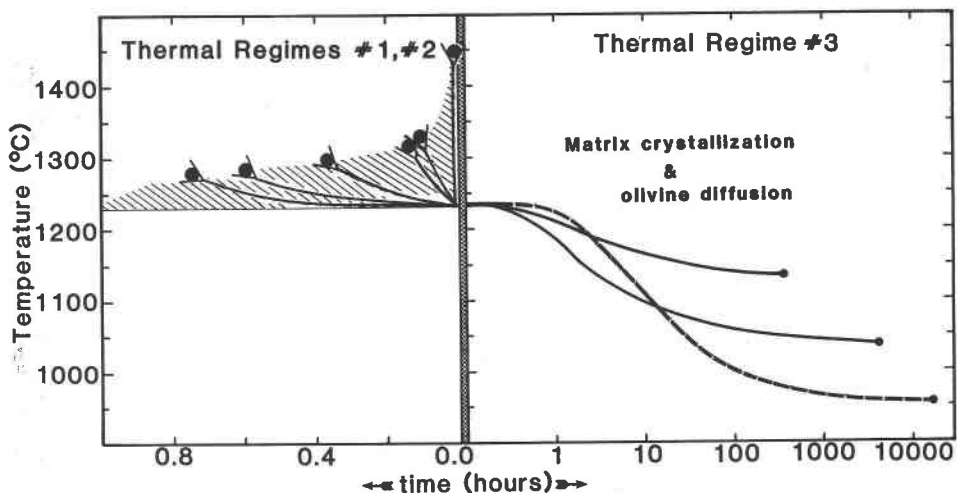


Fig. 10. Summary of the thermal history (temperature vs time) of lunar fragment-laden Basalt 77115 (see text). Left part of diagram illustrates temperature-time (linear) range of clast-melt thermal equilibration relative to the onset of crystallization. The right part depicts a range of cooling curves from near-liquidus temperatures.

metallic Fe may be relevant to the petrogenesis of Ni-Fe alloys in meteoritic, lunar, and terrestrial environments.

2. Compositional gradients in glass adjacent to crystals in isothermal resorption experiments are similar to those observed in natural samples and are a result of growth-related diffusion during quench.

3. The characterization of crystal/liquid interface textures in olivine-resorption experiments has provided a basis for recognition of olivine dissolution in igneous rocks, relevant to interpretation of histories of magmatic episodes. We hope that both the resorption-rate data and textural observations can be correlated with chemical and textural heterogeneity in natural samples and applied to an evaluation of the specific thermal and compositional disequilibria responsible for olivine dissolution.

The diversity of observations encountered in our investigation of the kinetics of olivine dissolution reflects the serendipitous nature of experimentation in an essentially unbroached aspect of igneous petrology. We think this area has large potential for future exploration.

Acknowledgments

This manuscript has benefited from the thoughtful reviews of M. P. Ryan and R. T. Helz (U.S. Geological Survey) and also T. L. Grove (Massachusetts Institute of Technology). The authors are grateful to R. T. Helz and to T. L. Grove for discussing and providing natural samples containing resorbed olivines. San Carlos olivines were given to CRT by Dan Schulze (Univ. Texas, Dallas). Discussions with J. Boland (Univ. Utrecht, the Netherlands) regarding enigmatic Fe-Ni precipitate in olivine were most informative. G. R. Robinson (U.S. Geological Survey) encouraged us to consider the mechanism of the resorption process and provided the senior author with helpful advice on the interpretation and presentation of results. Mary Woodruff (U.S. Geological Survey) provided technical assistance. This research was funded by NASA Contract T-781H.

References

- Albee, A. L., and Ray, L. (1970) Correction factors for electron probe microanalysis of silicates, oxides, carbonates, phosphates and sulfates. *Analytical Chemistry*, 42, 1408-1414.
- Anderson, A. T., Jr. (1974) Evidence for a picritic, volatile-rich magma beneath Mt. Shasta, California. *Journal of Petrology*, 15, 243-267.
- Bence, A. E., and Albee, A. L. (1968) Empirical correction factors for the electron microanalysis of silicates and oxides. *Journal of Geology*, 76, 382-403.
- Boland, J. N., and Duba, A. (1981) Solid-state reduction of iron in olivine-planetary and meteoritic evolution. *Nature*, 294, 142-144.
- Bowen, N. L., and Schairer, J. F. (1935) The system MgO-FeO-SiO₂. *American Journal of Science*, 29, 151-217.
- Buening, D. K., and Buseck, P. R. (1973) Fe-Mg lattice diffusion in olivine. *Journal of Geophysical Research*, 78, 6852-6862.
- Cawthorn, R. G., Ford, C. E., Biggar, G. M., Brava, M. S., and Clarke, D. B. (1973) Determination of the liquid composition in experimental samples: Discrepancies between microprobe analysis and other methods. *Earth and Planetary Science Letters*, 21, 1-5.
- Duba, A. (1976) Are laboratory conductivity data relevant to the Earth? *Acta Geodactica, Geophysica et Montanistica. Academiae Scientiarum Hungaricae*, 11, 485-495.
- Finger, L. W., and Hadidiacos, C. G. (1972) Electron microprobe automation. *Carnegie Institution of Washington Yearbook*, 71, 598-600.
- Freund, F., Kathrien, H., Wengeler, H., Knobel, R., and Heinen, H. J. (1980) Carbon in solid solution in forsterite—a key to the untractable nature of reduced carbon in terrestrial and cosmogenic rocks. *Geochimica et Cosmochimica Acta*, 44, 1319-1333.
- Gerlach, D. C., and Grove, T. L. (1983) Petrology of Medicine Lake highlands volcanics: Characterization of end-members of magma mixing. *Contributions to Mineralogy and Petrology*, 80, 147-159.
- Green, D. H. (1973) Experimental melting studies on a model

- upper mantle composition at high pressure under water-saturated and water-undersaturated conditions. *Earth and Planetary Science Letters*, 19, 37–53.
- Haggerty, S. E. (1976) Apollo 14: oxide, metal and olivine mineral chemistries in 14072 with a bearing on the temporal relationship of subsolidus reduction. Lunar Science Conference, 8th Proceedings, 1809–1829.
- Jarosewich, E., Nelen, J. A., and Norberg, J. A. (1979) Electron microprobe reference samples for mineral analysis. In R. F. Fudali, Ed., *Smithsonian Contributions to the Earth Sciences*, no. 22, p. 68–72.
- Kuo, L.-C. J. (1982) Kinetics of crystal dissolution in the system diopside–forsterite–anorthite. University of Illinois at Urbana-Champaign, Ph.D. thesis, 90 p.
- Kushiro, I. (1974) Melting of hydrous upper mantle and possible generation of andesitic magma: An approach from synthetic systems. *Earth and Planetary Science Letters*, 22, 294–299.
- Lofgren, G. E., Smith, D. P., and Brown, R. W. (1978) Dynamic crystallization and kinetic melting of the lunar soil. Lunar and Planetary Science Conference, 9th Proceedings, 959–975.
- Onorato, P. I. K., Uhlmann, D. R., and Simonds, C. H. (1978) The thermal history of the Manicouagan impact melt sheet, Quebec. *Journal of Geophysical Research*, 83, 2789–2798.
- Powell, M. A., Walker, D., and Hays, J. F. (1980) Controlled cooling and crystallization of a eucrite: Microprobe Studies. Lunar and Planetary Science Conference, 11th Proceedings, 1153–1168.
- Rambaldi, E. R., and Wasson, J. T. (1982) Fine, nickel-poor Fe–Ni grains in the olivine of unequilibrated ordinary chondrites. *Geochimica et Cosmochimica Acta*, 46, 929–939.
- Richter, D. H., and Murata, K. J. (1966) Petrography of the lavas of the 1959–60 eruption of Kilauea Volcano, Hawaii. U.S. Geological Survey Professional Paper 537-D.
- Roeder, P. L., and Emslie, R. F. (1970) Olivine–liquid equilibrium. *Contributions to Mineralogy and Petrology*, 29, 275–289.
- Sanford, R. F. (1982) Three fortran programs for finite difference solutions to binary diffusion in one and two phases with composition and time dependent diffusion coefficients. *Computers and Geosciences*, 8, 235–263.
- Sanford, R. F., and Huebner, J. S. (1980) Model thermal history of 77115 and implications for the origin of fragment-laden basalts. In Papike, J. J. and Merrill, R. B., Eds., *Proceedings of the Conference on Lunar Highlands Crust*, p. 253–269. Pergamon Press, New York.
- Sato, M. (1978) Oxygen fugacity of basaltic magmas and the role of gas-forming elements. *Geophysical Research Letters*, 5, 447–449.
- Sato, M., and Valenza, M. (1980) Oxygen fugacities of the layered series of the Skaergaard intrusion, East Greenland. *American Journal of Science*, 280-A, 134–158.
- Scarfe, C. M., Takahashi, E., and Yoder, H. S., Jr. (1980) Rates of dissolution of upper mantle minerals in an alkali-olivine basalt melt at high pressures. *Carnegie Institution of Washington Yearbook*, 79, 290–296.
- Simonds, C. H. (1975) Thermal regimes in impact melts and the petrology of the Apollo 17 Station 6 boulder. *Proceedings of the Lunar Science Conference*, 6th, 641–672.
- Thorner, C. R., and Haggerty, S. E., (1976) The origin and geochemistry of josephinite. *EOS (American Geophysical Union, Transactions)*, 57, 355.
- Thorner, C. R., and Huebner, J. S. (1980) An experimental study of the thermal history of fragment-laden “basalt” 77115. In Papike, J. J. and Merrill, R. B., Eds., *Proceedings of the Conference on Lunar Highlands Crust*, p. 233–252. Pergamon Press, New York.
- Thorner, C. R., and Huebner, J. S. (1982) Techniques for using iron crucibles in experimental igneous petrology. *American Mineralogist*, 67, 1144–1154.
- Wiggins, L. B., and Huebner, J. S. (1981) Combined X-ray wavelength and energy-dispersive analysis to increase microprobe efficiency. U.S. Geological Survey Open-File Report 81-1041.
- Wright, T. L. (1973) Magma mixing as illustrated by the 1959 eruption, Kilauea volcano, Hawaii. *Geological Society of America Bulletin* 84, 849–858.
- Yoder, H. S., and Sahara, T. G. (1957) Olivine X-ray determinative curve. *American Mineralogist*, 42, 475–491.

*Manuscript received, July 9, 1984;
accepted for publication, May 1, 1985.*